

# Mergers of accreting stellar-mass black holes

H. Tagawa<sup>1,2\*</sup>, M. Umemura<sup>3</sup>, and N. Gouda<sup>1,2</sup>

<sup>1</sup>*The University of Tokyo, 7-3-1 Hongo Bunkyo, Tokyo 113-0033, Japan*

<sup>2</sup>*National Astronomical Observatory of Japan, 2-21-1 Osawa, Mitaka, Tokyo 181-8588, Japan*

<sup>3</sup>*Center for Computational Sciences, University of Tsukuba, Tsukuba, Ibaraki 305-8577, Japan*

28 July 2016

## ABSTRACT

We present post-Newtonian  $N$ -body simulations on mergers of accreting stellar-mass black holes (BHs), where such general relativistic effects as the pericenter shift and gravitational wave (GW) emission are taken into consideration. The attention is concentrated on the effects of the dynamical friction and the Hoyle-Lyttleton mass accretion by ambient gas. We consider a system composed of ten BHs with initial mass of  $30 M_{\odot}$ . As a result, we show that mergers of accreting stellar-mass BHs are classified into four types: a gas drag-driven, an interplay-driven, a three body-driven, or an accretion-driven merger. We find that BH mergers proceed before significant mass accretion, even if the accretion rate is  $\sim 10$  Eddington accretion rate, and then all BHs can merge into one heavy BH. Using the simulation results for a wide range of parameters, we derive a critical accretion rate ( $\dot{m}_c$ ), below which the BH growth is promoted faster by mergers. Also, it is found that the effect of the recoil by the GW emission can reduce  $\dot{m}_c$  especially in gas number density higher than  $10^8 \text{ cm}^{-3}$ , and enhance the escape probability of merged BHs. Very recently, a gravitational wave event, GW150914, as a result of the merger of a  $\sim 30 M_{\odot}$  BH binary has been detected (Abbott et al. 2016). Based on the present simulations, the BH merger in GW150914 is likely to be driven by three-body encounters accompanied by a few  $M_{\odot}$  of gas accretion, in high-density environments like dense interstellar clouds or galactic nuclei.

**Key words:** stars: black holes – gravitational waves – dark ages, reionization, first stars – galaxies: high-redshift – galaxies: nuclei – quasars: supermassive black holes.

## 1 INTRODUCTION

Recent observations have revealed the existence of supermassive black holes (SMBHs) with masses  $\gtrsim 10^9 M_{\odot}$  at redshifts higher than 6 (Fan et al. 2001; Kurk et al. 2007; Mortlock et al. 2011; Wu et al. 2015). However, the formation history of these SMBHs is not still revealed. There are two major competitive scenarios for the growth of SMBHs: one is the mass accretion, and the other is the merger of BHs (or stars) (Volonteri & Bellovary 2012; Haiman 2013). As for the mass accretion, the constraints from observed SMBHs at high redshifts have been argued. Possible building blocks of SMBHs are the remnants of first stars. First stars of several tens  $M_{\odot}$  can leave black holes (BHs) of few tens  $M_{\odot}$  after supernova explosion (Heger & Woosley 2002). If recently discovered high-redshift quasars, ULASJ112010+641 with the mass of  $m_{\text{BH}} = 2 \times 10^9 M_{\odot}$  at redshift  $z = 7.085$  (Mortlock et al. 2011) and SDSS J01001+2802 with  $m_{\text{BH}} =$

$1.2 \times 10^{10} M_{\odot}$  at  $z = 6.30$  (Wu et al. 2015), grow via mass accretion from such stellar-mass BHs, the Eddington ratio ( $\lambda$ ) is required to be  $\lambda = 1.4$  for ULASJ112010+641, or  $\lambda = 1.3$  for SDSS J01001+2802. However, the continuous accretion is unlikely to be sustained due to feedback, and thus the average mass accretion rates should be lower than the Eddington rate (Alvarez, Wise, & Abel 2009; Milosavljevic, Couch & Bromm 2009), although it is pointed out that the super-Eddington accretion may be allowed in metal free systems (Volonteri & Rees 2005). The maximum rate of the super-Eddington accretion is thought to be given by Hoyle-Lyttleton accretion (Hoyle & Lyttleton 1939; Bondi & Hoyle 1944). However, it is not elucidated how high accretion rate is realized in an early universe.

On the other hand, according to the hierarchical merger history of galaxy formation, galaxies with multiple MBHs are likely to form, if the number of BHs is conserved during the galaxy merger. However, most of galaxies harbor just one SMBH in their centres, with several exceptions like a triple AGN in the galaxy SDSS J1027+1749 at

\* E-mail: email@address ; tagawahr@nao.ac.jp

$z = 0.066$  (Liu, Shen & Strauss 2011), three rapidly growing MBHs of  $10^6 - 10^7 M_\odot$  in a clumpy galaxy at  $z = 1.35$  (Schawinski et al. 2011), a quasar triplet QQQJ1432–0106 at  $z = 2.076$  (Djorgovski et al. 2007), and a second quasar triplet QQQJ1519+0627 at  $z = 1.51$  (Farina et al. 2013). Thus, it is conceivable that the merger of BHs might take place in some redshift epoch, resultantly forming one central SMBH.

The merger of massive BHs may be a potential source of gravitational waves for the Laser Interferometer Space Antenna (LISA) and pulsar timing (Berti, Cardoso, & Will 2006; Sesana et al. 2005; Wyithe & Loeb 2003). Also, the inspiral, merger, and ringdown of binary stellar-mass black hole systems can be demonstrated by gravitational waves with the Laser Interferometer Gravitational-Wave Observatory (LIGO), the VIRGO (Abbott et al. 2006; Aasi et al. 2013), the EGO 600 (Lück et al. 2006), or the KAGRA (Aso et al. 2013). Very recently, the first example of gravitational waves from the merger of a  $36M_\odot$  and  $29M_\odot$  BH binary has been detected in the LIGO (Abbott et al. 2016). These observations show that binary stellar-mass black hole systems do exist and they can merge due to gravitational wave radiation within the cosmic time. Also, a weak hard X-ray transient source was detected at 0.4 s after the GW event with *Fermi* Gamma-ray Burst Monitor (Connaughton et al. 2016).

Recent radiation hydrodynamic simulations on the formation of first stars show that multiple massive stars form in a primordial gas cloud of  $\sim 10^4 - 10^5 M_\odot$  with the density of around  $10^7 \text{ cm}^{-3}$  and the extension of  $\sim 0.01 \text{ pc}$ , where the gas fraction is 99% (Greif et al. 2011; Umemura et al. 2012; Susa 2013; Susa, Hasegawa, & Tominaga 2014). According to the mass function of first stars, multiple BHs of several tens  $M_\odot$  may be born as remnants of supernovae, in such a primordial cloud. In this circumstance, high mass-accretion rates onto BHs are expected. On the other hand, plenty of gas can exert dynamical friction on moving BHs. Recently, Tagawa et al. (2015) has explored the early merger of BHs through the gas dynamical friction, and have shown that the merger time of multiple BHs merger in the gas number density of  $n_{\text{gas}} \gtrsim 10^6 \text{ cm}^{-3}$  is  $\sim 10^7 \text{ yr}$ , which is shorter than the Eddington timescale. However, Tagawa et al. (2015) did not consider the effect of the mass accretion onto BHs. Thus, in the competition between the mass accretion and the merger, which mechanism dominates the growth of massive BHs is not clear.

In this paper, we simulate a multiple BH system, including both the gas dynamical friction and the gas accretion, and derive the critical condition that bifurcates the key mechanism of the growth of BHs. In Section 2, we describe the method for numerical simulations. In Section 3, numerical results on merger mechanisms are presented. In Section 4, we derive the critical condition that determines a predominant merger mechanism, and discuss related issues, including the GW150914 event. Section 5 is devoted to conclusions.

## 2 METHOD FOR NUMERICAL SIMULATIONS

### 2.1 Numerical scheme

Tagawa et al. (2015) gives a detailed description of the simu-

lation used here. We summarize some important treatments in our simulations.

The equations of motion for BHs are given by

$$\frac{d^2 \mathbf{r}_i}{dt^2} = \sum_j^{N_{\text{BH}}} \left\{ -Gm_j \frac{\mathbf{r}_i - \mathbf{r}_j}{|\mathbf{r}_i - \mathbf{r}_j|^3} + \mathbf{a}_{\text{PN},ij} \right\} + \mathbf{a}_{\text{acc},i} + \mathbf{a}_{\text{DF},i}^{\text{gas}} + \mathbf{a}_{\text{pot},i}, \quad (1)$$

where  $\mathbf{r}_i$  and  $\mathbf{r}_j$  are respectively the positions of  $i$ -th BH and  $j$ -th BH,  $N_{\text{BH}}$  is the number of BHs,  $G$  is the gravitational constant,  $m_j$  is the mass of  $j$ -th BH,  $\mathbf{a}_{\text{PN},ij}$  is the general relativistic acceleration of  $j$ -th BH on  $i$ -th BH in the post-Newtonian prescription up to 2.5PN term (Kupi 2006). 1PN and 2PN terms correspond to the pericenter shift, and 2.5PN term does to the gravitational wave (GW) emission.  $\mathbf{a}_{\text{acc},i}$  is the acceleration of  $i$ -th BH due to the gas accretion,  $\mathbf{a}_{\text{DF},i}^{\text{gas}}$  is the acceleration of the dynamical friction (DF) on  $i$ -th BH by gas, and  $\mathbf{a}_{\text{pot},i}$  is the acceleration on  $i$ -th BH by gravitational potential of gas.

For the gas dynamical friction force, we use the formula given by Tanaka & Haiman (2009) for the motion with  $\mathcal{M}_i < \mathcal{M}_{\text{eq}}$  and Ostriker (1999) for  $\mathcal{M}_i > \mathcal{M}_{\text{eq}}$ , where  $\mathcal{M}_i$  is the Mach number of  $i$ -th BH and  $\mathcal{M}_{\text{eq}}$  is the Mach number where these two formulas give equal acceleration. Here, we adopt  $\mathcal{M}_{\text{eq}} = 1.5$  as Tanaka & Haiman (2009). Then, the acceleration of the gas dynamical friction ( $\mathbf{a}_{\text{DF},i}^{\text{gas}}$ ) is given by

$$\mathbf{a}_{\text{DF},i}^{\text{gas}} = -4\pi G^2 m_i m_{\text{H}} n_{\text{gas}}(r) \frac{\mathbf{v}_i}{v_i^3} \times f(\mathcal{M}_i) \quad (2)$$

$$f(\mathcal{M}_i) = \begin{cases} 0.5 \ln \left( \frac{v_i t}{r_{\text{min}}} \right) \left[ \text{erf} \left( \frac{\mathcal{M}_i}{\sqrt{2}} \right) - \sqrt{\frac{2}{\pi}} \mathcal{M}_i \exp \left( -\frac{\mathcal{M}_i^2}{2} \right) \right], & (0 \leq \mathcal{M}_i \leq 0.8) \\ 1.5 \ln \left( \frac{v_i t}{r_{\text{min}}} \right) \left[ \text{erf} \left( \frac{\mathcal{M}_i}{\sqrt{2}} \right) - \sqrt{\frac{2}{\pi}} \mathcal{M}_i \exp \left( -\frac{\mathcal{M}_i^2}{2} \right) \right], & (0.8 \leq \mathcal{M}_i \leq \mathcal{M}_{\text{eq}}) \\ \frac{1}{2} \ln \left( 1 - \frac{1}{\mathcal{M}_i^2} \right) + \ln \left( \frac{v_i t}{r_{\text{min}}} \right), & (\mathcal{M}_{\text{eq}} \leq \mathcal{M}_i) \end{cases} \quad (3)$$

where  $m_{\text{H}}$  is the mass of the hydrogen atom,  $n_{\text{gas}}$  is the number density of gas,  $v_i$  is the velocity of  $i$ -th BH, and  $t$  is the elapsed time. The  $r_{\text{min}}$  is the minimum scale of the dynamical friction on a BH, and we give  $r_{\text{min}}$  as  $Gm_i/v_i^2$ . Here,  $v_i t$  means the effective scale of gas medium, and we set an upper limit of  $v_i t$  to 0.1 pc. When  $v_i t < r_{\text{min}}$ , we assume  $f(\mathcal{M}_i) = 0$ .

The equations of motion is integrated using the fourth-order Hermite scheme with the shared time step (Makino & Aarseth 1992) whose accuracy parameter is set to be 0.003. To use the fourth-order Hermite scheme, we calculate the time derivative of the acceleration by the Newtonian gravity, the gas gravitational potential, and the relativistic force. On the other hand, we treat the dynamical friction and the accretion of gas to quadratic order.

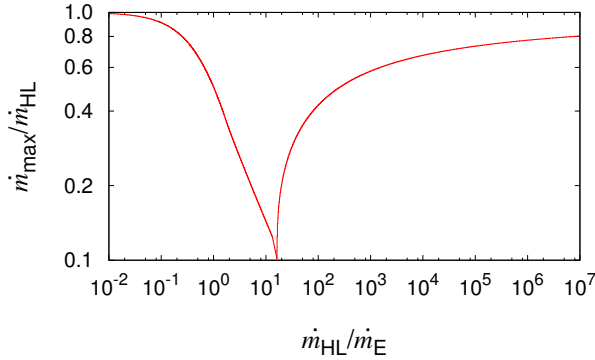


**Figure 1.** The maximum gas accretion rate ( $\dot{m}_{\max}$ ) with the reduction by radiation pressure as a function of the Eddington accretion rate ( $\dot{m}_{\text{E}}$ ), where  $\dot{m}_{\text{HL}}$  is the Hoyle-Lyttleton accretion rate. A viscous accretion disk with viscosity parameter  $\alpha = 0.1$  is assumed.

## 2.2 Mass accretion rate

We envisage the Hoyle-Lyttleton accretion onto BHs. The mass accretion rate is not limited by the Eddington luminosity in a BH accretion disk, since photons are trapped in innermost optically-thick regions without diffusing out from the disk surface (so-called photon trapping effects) (Abramowicz et al. 1988). Here, we employ a model for such a super-Eddington accretion. The luminosity of a super-Eddington disk is fitted as

$$\Gamma \equiv L/L_{\text{E}} \approx \begin{cases} 2 \left[ 1 + \ln \left( \frac{\dot{m}}{20\eta\dot{m}_{\text{E}}} \right) \right] & \text{for } \dot{m} \geq 20 \eta\dot{m}_{\text{E}} \\ \left( \frac{\dot{m}}{10\eta\dot{m}_{\text{E}}} \right) & \text{for } \dot{m} < 20 \eta\dot{m}_{\text{E}} \end{cases} \quad (4)$$

for the viscosity parameter  $\alpha = 0.1$  (Watarai et al. 2000), where  $L_{\text{E}}$  is the Eddington luminosity,  $\dot{m}$  is the mass accretion rate,  $\dot{m}_{\text{E}} (= L_{\text{E}}/\eta c^2)$  is the Eddington accretion rate,  $\eta$  is the radiative energy conversion efficiency ( $\eta = 0.1$  in this paper), and  $c$  is the light speed.

Also, we take the effect of the radiation pressure on the Hoyle-Lyttleton accretion into consideration. The accretion rate is reduced due to the radiation pressure as

$$\frac{\dot{m}}{\dot{m}_{\text{HL}}} = \begin{cases} (1 - \Gamma) & (0 \leq \Gamma \leq 0.64) \\ (1 - \Gamma - \frac{2}{\pi}\psi_0 + \Gamma \sin\psi_0) & (0.64 \leq \Gamma \leq 1.65) \\ \frac{2}{\pi} \tan^{-1} \left( \frac{\Gamma}{0.75 \ln 10^5} \right) & (1.65 \leq \Gamma) \end{cases} \quad (5)$$

(Hanamoto, Ioroi & Fukue 2001), where  $\dot{m}_{\text{HL}}$  is the Hoyle-Lyttleton accretion rate, and  $\cos\psi_0 = 2/(\pi\Gamma)$ . By combining equations (4) and (5), we can derive the maximum gas accretion rate ( $\dot{m}_{\max}$ ), which is shown in Fig. 1. This figure shows that the Hoyle-Lyttleton accretion rate is maximally reduced down to  $\sim 0.1 \dot{m}_{\text{HL}}$  around  $\dot{m}_{\text{E}}/\dot{m}_{\text{HL}} \approx 10$ . For  $\dot{m}_{\text{E}}/\dot{m}_{\text{HL}} > 10$ , the reduction is alleviated owing to the photon trapping effect.

To parameterize the accretion rate, we set the gas mass accretion rate as

$$\dot{m}_i = \epsilon \dot{m}_{\text{HL},i} = \epsilon \frac{4\pi G^2 m_{\text{H}} n_{\text{gas}} m_i^2}{(C_s^2 + v_i^2)^{3/2}}, \quad (6)$$

where  $v_i$  is the velocity of  $i$ th BH, and  $\epsilon (\leq 1)$  is the accretion

efficiency. In this paper, taking another feedback effects into consideration, we consider the range of  $10^{-7} \leq \epsilon \leq 1$ . For a given  $\dot{m}_i$ , it is limited to the maximum accretion rate. As for the back reaction by gas accretion, we incorporate the acceleration due to mass accretion. If we assume the relative velocity between gas and BH to be the BH velocity (i.e., static ambient gas on the Hoyle-Lyttleton accretion scales), the acceleration due to mass accretion on  $i$ th BH  $a_{\text{acc},i}$  is given as

$$a_{\text{acc},i} = -\frac{\dot{m}_i v_i}{m_i}. \quad (7)$$

Also, when the gas accretes onto BHs, we lessen the gas mass and correspondingly the gas number density to conserve the total mass of the system.

## 2.3 Setup of Simulations

One key parameter in our simulations is the BH density,  $\rho_{\text{BH}}$ , at the initial epoch. Recent radiation hydrodynamic simulations on the formation of the first stars have shown that several or more stars are born in a disk of  $\sim 0.01$  pc (Greif et al. 2011; Umemura et al. 2012; Susa 2013; Susa, Hasegawa, & Tominaga 2014). Referring to these results, we change the typical extensions of BH distributions at the initial epoch,  $r_{\text{typ}}$ , to settle the BH density. We investigate the range from 0.01 pc to 0.1 pc in this paper. As first star remnants, we set up ten BHs of equal mass of  $30 M_{\odot}$  initially.

Another key parameter is the gas number density  $n_{\text{gas}}$ . Simulations of first star formation show that  $n_{\text{gas}}$  is  $\sim 10^{7-8} \text{ cm}^{-3}$  in a primordial cloud of  $\sim 0.01$  pc. In this paper, we consider a wider range of the gas density to explore the possibility of BH mergers in a wide variety of environments. In dense interstellar cloud cores,  $n_{\text{gas}}$  ranges from  $10^5 \text{ cm}^{-3}$  to  $10^7 \text{ cm}^{-3}$  (e.g. Bergin, Snell, & Goldsmith 1996). In galactic nuclear regions,  $n_{\text{gas}} \gtrsim 10^8 \text{ cm}^{-3}$  at  $\lesssim 1$  pc (e.g. Namekata & Umemura 2016). Anyhow the gas density is less than  $10^{10} \text{ cm}^{-3}$  in realistic environments, but we consider even higher densities up to  $10^{12} \text{ cm}^{-3}$  as well in order to elucidate more clearly the dependence of merger criteria on the gas density.

Although Tagawa et al. (2015) assumed that gas is distributed infinitely, we settle the finite gas mass in a sphere with  $M_{\text{gas,tot}} = 10^5 M_{\odot}$  in this paper. Outside this sphere, BHs are not subject to gas dynamical friction and gas accretion. In realistic environments, the density distributions of gas are likely to be fairly complex. In first-generation objects, the axis ratios of gas disks ranges from one to five (Hirano et al. 2014), and also the gas flow by cold accretion along filaments may change the gas distribution significantly at high redshifts (e.g. Yajima et al. 2015). In dense molecular cloud cores, the gas distributions are sometimes fairly spherical and sometimes elongated. Since the gas distributions depend on objects of interest, we assume a spherical cloud in this paper just for simplicity. The temperature of the gas is set to be 1000 K, based on the thermal history of the metal poor gas (Omukai 2000). Consequently, the sound speed is given as  $C_s = 3.709$  [km/s]. Furthermore, we change the gas accretion efficiency,  $\epsilon$ , as an important parameter, which is constrained as described in the previous section. Since gas accretion rate in a first-generation object is not

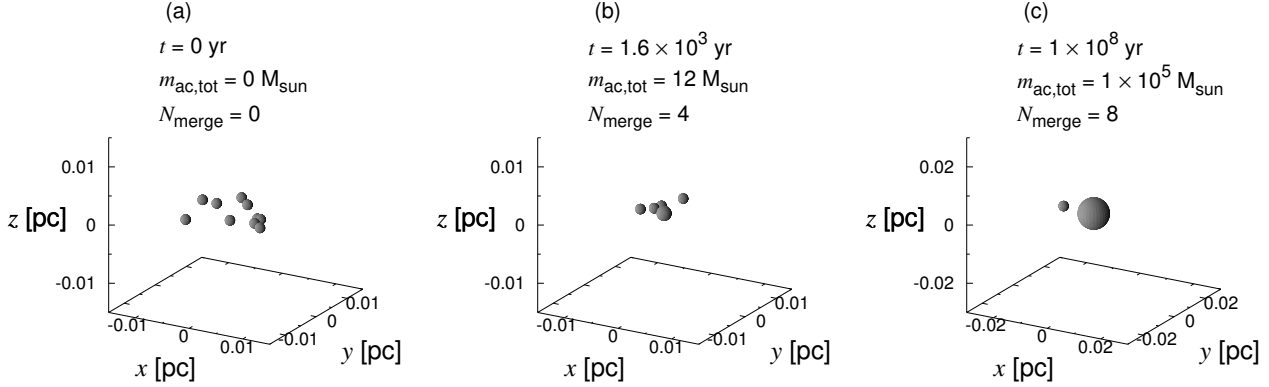


**Figure 2.** Snapshots of the distributions of the multiple BHs for a gas drag-driven merger (type A). The initial parameters are a typical extension of BH distributions,  $r_{\text{typ}} = 0.01$  pc, the gas number density,  $n_{\text{gas}} = 10^{12}$  cm $^{-3}$ , and the accretion efficiency,  $\epsilon = 10^{-4}$ . In each snapshot, the elapsed time  $t$ , the total accreted mass  $m_{\text{ac,tot}}$  onto BHs, and the number of merged BHs  $N_{\text{merge}}$  are presented. The sizes of spheres represent the mass of the BH in logarithmic scales, where the smallest one corresponds to the initial BH mass,  $m_i = 30M_{\odot}$ .

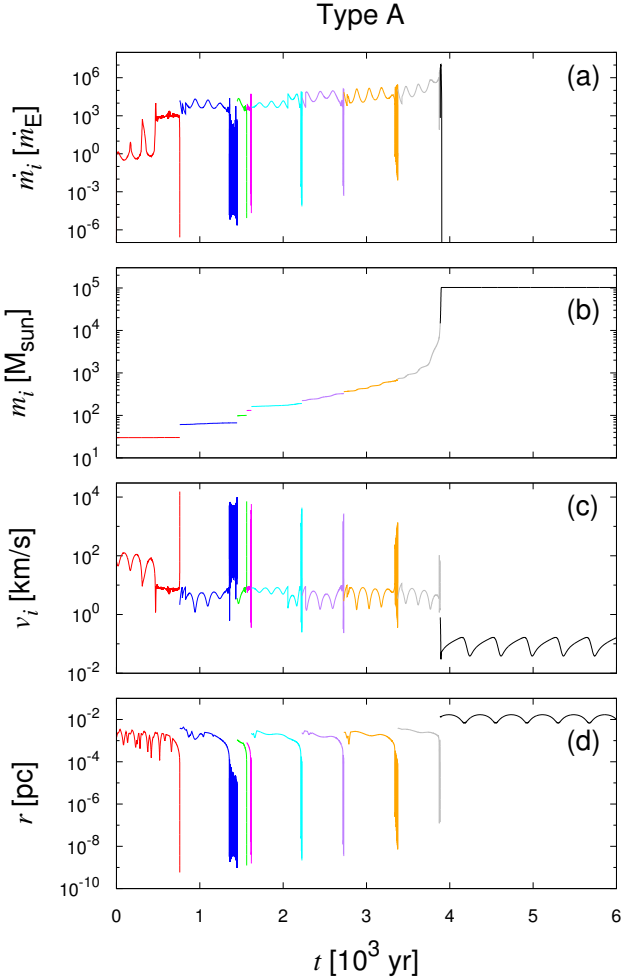


**Figure 3.** The time evolution of the physical quantities for a gas drag-driven merger (type A). The initial parameters are the same as Figure 2. Panels (a), (b), and (c) represent the mass accretion rate in units of the Eddington mass accretion rate for  $30M_{\odot}$ , the mass and the velocity of the first merged BH, respectively. Panel (d) represents the separation of the closest pair within all BHs, where the colors of lines change at every event of the BH merger.

elucidated, we study a wider range of gas accretion rate as  $\epsilon$  from  $10^{-7}$  to 1.

We assume that two MBHs merge, when their separation is less than 100 times the sum of their Schwarzschild radii:

$$|\mathbf{r}_i - \mathbf{r}_j| < 100 (r_{\text{sch},i} + r_{\text{sch},j}), \quad (8)$$

where  $r_{\text{sch},i}$  is the Schwarzschild radius of  $i$ -th BH given by  $2Gm_i/c^2$  with the speed of light  $c$ . Therefore, the simulations do resolve the scales of  $100 r_{\text{sch}} = 2 \times 10^9$  cm. To avoid cancellation of significant digits when such tiny scales as  $100 r_{\text{sch}}$  are resolved, the BHs evolution is calculated in the coordinate, where the origin is always set to the center of mass for the closest pair of BHs. This prescription allows us to pursue accurately the orbit of the BHs until the merger condition is satisfied. At the final stage of merger, the binding energy of a binary BH is transformed to the energy of GW, retaining the mass of each BH.

We give the initial positions of BHs randomly in the  $x - y$  plane within  $r_{\text{typ}}$ . Also, the velocity of each BH is given as the sum of a circular component and a random component. The circular velocity is given to balance against the gravity of gas in the  $x - y$  plane. Besides, we give the random velocity in the  $xyz$  space according to a Gaussian distribution with the same dispersion as the circular velocity.

Our simulations are performed for 100 Myr, since the background environments of the host objects are likely to change in 100 Myr. Also, we terminate the simulation, if all BHs merge into one BH, or if all other BHs are escaped except one BH.

### 3 MERGER MECHANISMS

Here, we present the merger mechanisms depending upon the gas density and accretion rate. In our previous study without mass accretion (Tagawa et al. 2015), the merger mechanisms are categorized into three types: a gas drag-driven merger (type A), an interplay-driven merger (type B), and a three body-driven merger (type C). In this study, we find an additional merger mechanism, which is referred

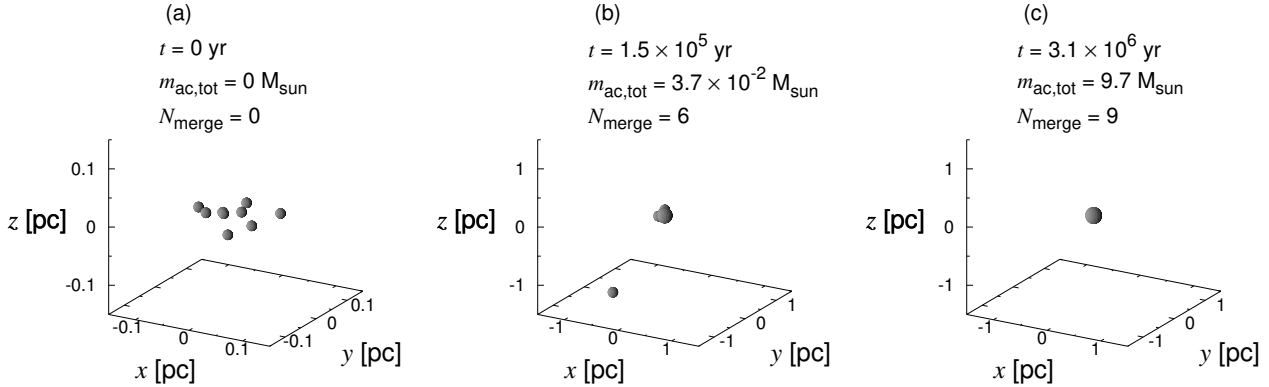


**Figure 4.** Same as Fig. 2, but for an interplay-driven merger (type B).  $r_{\text{typ}} = 0.1$  pc,  $n_{\text{gas}} = 10^9$  cm $^{-3}$ , and  $\epsilon = 10^{-6}$ .

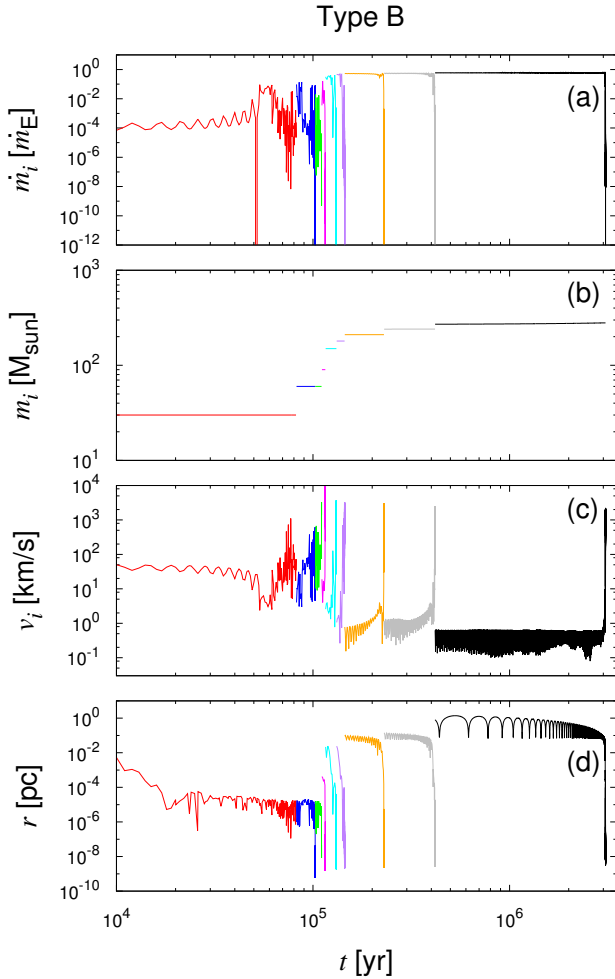


**Figure 5.** Same as Fig. 3, but for an interplay-driven merger (type B).  $r_{\text{typ}} = 0.1$  pc,  $n_{\text{gas}} = 10^9$  cm $^{-3}$ , and  $\epsilon = 10^{-6}$ .

to as an accretion-driven merger (type D). The classification is based on the manner of orbit decay just before the gravitational wave emission drives the merger. In type A, the orbit is decayed due to the dynamical friction by gas before the gravitational wave works. In both of types B and C, the strong disturbance of the orbit is induced by three-body in-

teraction during the first merger. But in type B, after first few mergers that are promoted by three-body interactions, the separations of BHs are increased due to the slingshot mechanism. Thereafter, the orbits of BHs decay slowly for long time through the gas dynamical friction. Whether the slow mergers occur from increased separations is the criterion on which type B is discriminated from type C. In type C, the strong disturbance of the orbit due to three-body interactions continues until the final merger. In type D, significant accretion occurs before the first merger. In the following, we scrutinize the effects of gas accretion on each merger mechanism.

### 3.1 Gas drag-driven merger (type A)

In Fig. 2, the snapshots of the distributions of multiple BHs for a gas drag-driven merger (type A) are shown in three different stages, where a typical extension of BH distributions is initially  $r_{\text{typ}} = 0.01$  pc, the background gas number density is as high as  $n_{\text{gas}} = 10^{12}$  cm $^{-3}$ , and the accretion efficiency is  $\epsilon = 10^{-4}$ . The sizes of spheres represent the mass of the BH in logarithmic scales, where the smallest one corresponds to the initial BH mass,  $m_i = 30M_{\odot}$ . In each snapshot, the elapsed time  $t$ , the total accreted mass  $m_{\text{ac,tot}}$  onto BHs, and the number of merged BHs  $N_{\text{merge}}$  are presented. As shown in this figure, several BHs merge without considerable mass accretion before  $1.6 \times 10^3$  yr. Thereafter, subsequent mergers proceed and eventually all gas accretes onto the most massive BH before  $10^8$  yr.

To see the detailed physical processes, we present, in Fig. 3, the time evolution of the mass accretion rate, the mass and the velocity of the first merged BH, and the separation of the closest pair within all BHs. In a type A merger, the separation of BHs decays effectively due to the dynamical friction (DF). The DF timescale is given by

$$t_{\text{DF}} \simeq \frac{v^3}{4\pi G^2 m_{\text{BH}} m_{\text{H}} n_{\text{gas}}}. \quad (9)$$

On the other hand, the accretion timescale, at which the accretion rate diverges, is given as

$$t_{\text{ac}} = \frac{(v^2 + C_s^2)^{3/2}}{4\pi G^2 m_{\text{BH}} m_{\text{H}} n_{\text{gas}} \epsilon}. \quad (10)$$

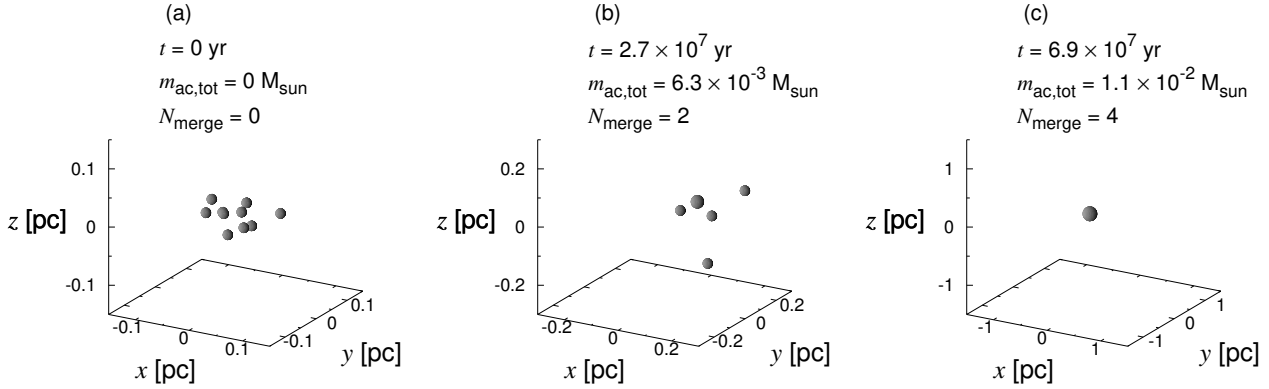


**Figure 6.** Same as Fig. 2, but for a three-body-driven merger (type C).  $r_{\text{typ}} = 0.1$  pc,  $n_{\text{gas}} = 10^6$  cm $^{-3}$ , and  $\epsilon = 10^{-6}$ .

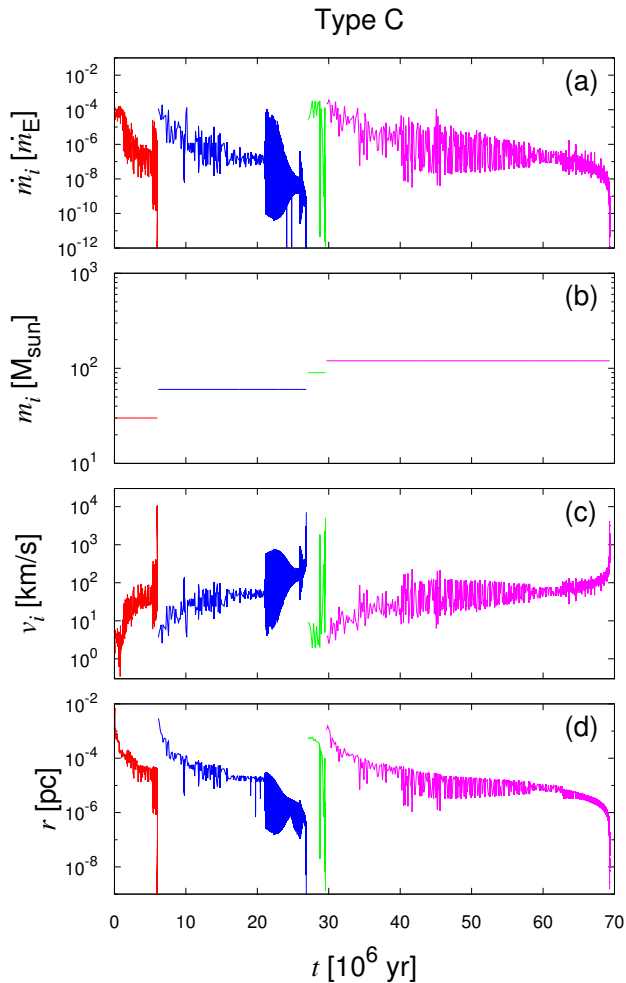


**Figure 7.** Same as Fig. 3, but for a three-body-driven merger (type C).  $r_{\text{typ}} = 0.1$  pc,  $n_{\text{gas}} = 10^6$  cm $^{-3}$ , and  $\epsilon = 10^{-6}$ .

It is noted that the accretion timescale has the same dependence as the DF timescale on the BH mass and the gas density, because the Hoyle-Lyttleton accretion and the DF are both caused by the change of the streamline due to the gravity of a BH. However, the velocity-dependence is different from each other. The accretion timescale is longer

than the DF timescale, since the accretion timescale depends on the sound velocity and also on the accretion efficiency  $\epsilon$  ( $\leq 1$ ). But, as in the first merger shown in Fig. 3, the accretion timescale is regardless of the sound speed, if the velocity is supersonic (panel (c)). On the other hand, the accretion timescale is increased by a low accretion efficiency as  $\epsilon = 10^{-4}$ . Therefore, the decay of orbit is predominantly driven by the gas dynamical friction (panel (d)) before significant gas accretion. As a result, a close BH binary forms and eventually merges into one BH due to the gravitational wave radiation before  $10^3$  yr. Thereafter, although there is a long phase when the BH velocity is low and the accretion rate is accordingly raised, the DF timescale is still shorter than the accretion timescale. Hence, successive mergers proceed by the dynamical friction. It is worth noting that the velocity is highly supersonic at the moment of merger owing to the inspiral by friction and therefore the accretion rate is much lower than the Eddington rate. Finally, when all gas instantly accretes onto the most massive BH, the merger stops and a binary BH is left in the system as seen in panel (c) of Fig. 2.

### 3.2 Interplay-driven merger (type B)

An example of an interplay-driven merger (type B) is presented in Fig. 4 and Fig. 5. In this example, the accretion efficiency is as low as  $\epsilon = 10^{-6}$ . As seen in panel (d) of Fig. 5, strong irregular oscillations of the separation of BHs occur in the first several mergers. If they are simply the Keplerian orbital motions of a binary, both of the pericenter and apocenter shrink smoothly due to the gas drag. However, in Fig 5, the pericenter and apocenter change promptly many times in the first few mergers. Such discontinuous changes of the pericenter and apocenter are typical in the three-body encounters. Hence, the successive mergers are thought to be promoted by the three-body interaction. On the other hand, in the last few mergers, the orbital evolution starts from a larger separation than the initial typical separation and the separation of BHs decays smoothly due to the dynamical friction. This increase of separation is a negative effect of three-body interaction. The panel (b) of Fig. 4 shows that a BH is kicked out due to slingshot mechanism. As a result of this negative effect, the velocity becomes much

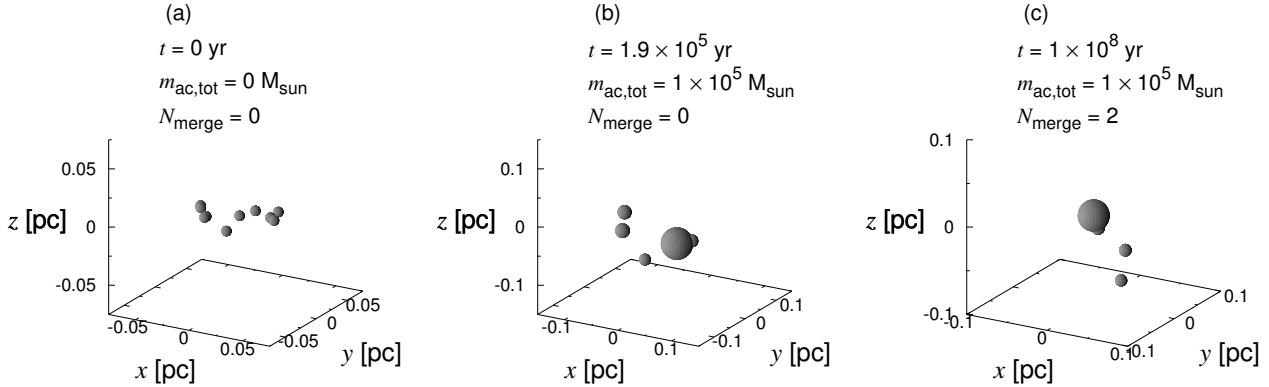


**Figure 8.** Same as Fig. 2, but for an accretion-driven merger (type D).  $r_{\text{typ}} = 0.04$  pc,  $n_{\text{gas}} = 10^7$  cm $^{-3}$ , and  $\epsilon = 10^{-1}$ .

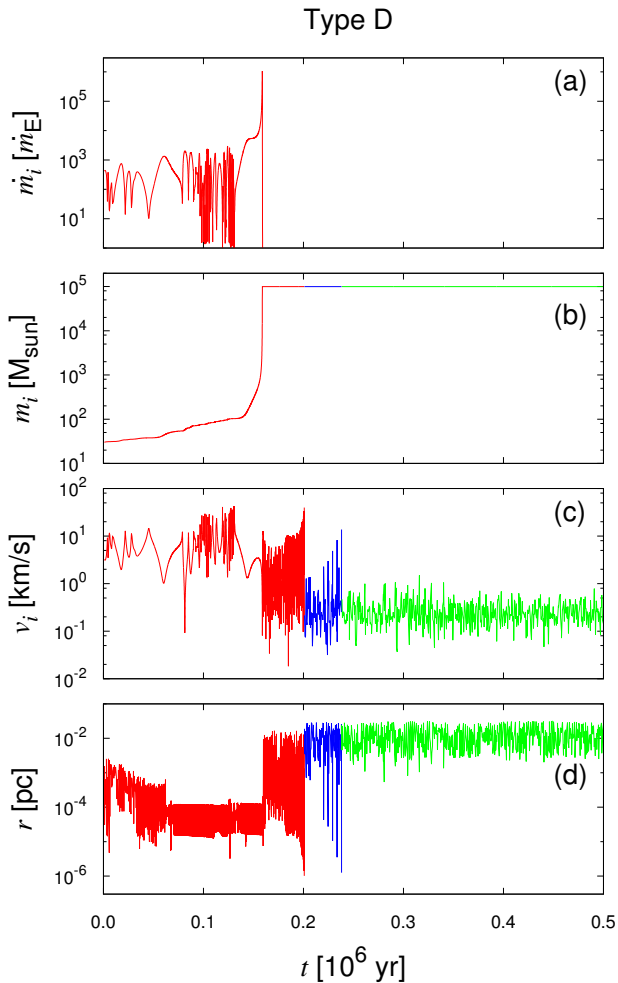


**Figure 9.** Same as Fig. 3, but for an accretion-driven merger (type D).  $r_{\text{typ}} = 0.04$  pc,  $n_{\text{gas}} = 10^7$  cm $^{-3}$ , and  $\epsilon = 10^{-1}$ .

lower than the sound velocity due to the deceleration by the gas potential (see panel (c) in Fig. 5), so that the accretion rate is raised in the later phase. However, mergers by the dynamical friction proceed faster than the accretion, because the accretion efficiency is quite low compared to the

Hoyle-Lyttleton accretion. Eventually, all BHs merge into one within  $3 \times 10^6$  yr, and all the accreted mass is  $9.7M_{\odot}$ .

### 3.3 Three body-driven merger (type C)

In a three body-driven merger (type C), the strong disturbance of the orbit continues until the final merger. The three-body interaction of BHs solely transfers the angular momentum, eventually causing the merger via the gravitational wave radiation. An example of type C is presented in Fig. 6 and Fig. 7. The initial parameters are the same as those in the above type B merger, excepting for lower background gas density. Strong oscillations of separation of BHs seen in panels (c) and (d) of Fig. 7 are caused by the three-body encounters. In a type C, since each BH of a closest pair receives the gravity mainly from another BH, the velocities of BHs in a closest pair increase according to the decay of the separation through three-body interactions, keeping supersonic velocities. Therefore, the accretion rates of the BHs of closest pair for type C are much lower than those in a type B. On the other hand, several BHs are kicked out from the central regions due to the slingshot mechanism before the first few mergers, and eventually a few BHs escape from the system. These escaping BHs are decelerated by the gas gravity, and therefore the velocities become as low as the sound velocity. The accretion rates onto these escaping BHs are often higher than those of the BHs of closest pair, but they never join the mergers of BHs. As a result, only multiple BHs left in the system merge into one BH.

### 3.4 Accretion-driven merger (type D)

In an accretion-driven merger (type D), significant accretion occurs before the first merger. A type D emerges with a high accretion rate near to the Hoyle-Lyttleton rate. Fig. 9 shows a typical evolution in a type D. In this model, the mass accretion is not high on the closest pair of BHs, because the accretion rate is reduced by their high circular velocities, according to equation (6). Instead, an isolated BH, which has low velocity and drifts in the outer regions for long time, grows first by accretion. In Fig. 9, the accretion rate, growth of mass, and velocity of the heaviest BH are shown. In this model, the BH swallows almost all gas during the drift with

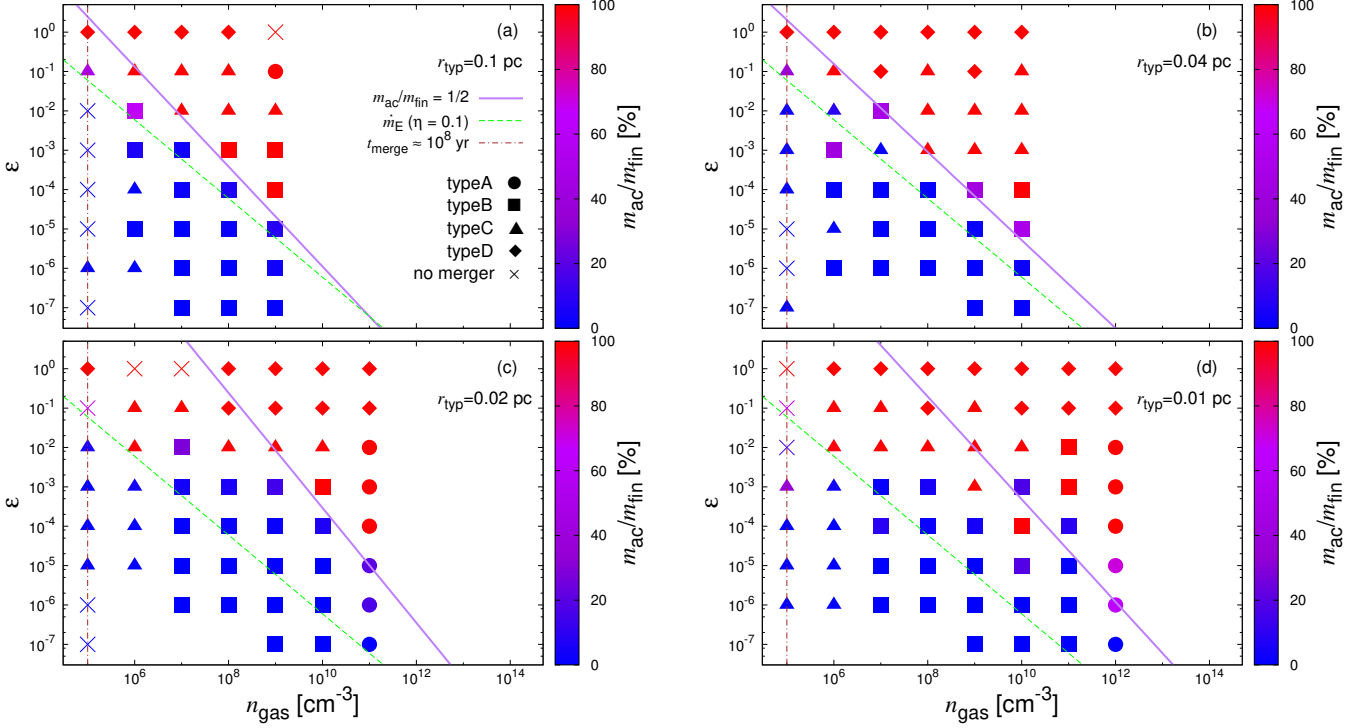


**Figure 10.** The contribution of the accreted mass to the final mass of the most massive BH as functions of the gas density ( $n_{\text{gas}}$ ) and the accretion efficiency ( $\epsilon$ ). Filled circles, squares, triangles, diamonds, and crosses represent gas drag-driven mergers (type A), interplay-driven mergers (type B), three body-driven mergers (type C), accretion-driven mergers (type D), and no merger, respectively. The initial typical extension of BH distributions is (a)  $r_{\text{typ}} = 0.1$  pc, (b) 0.04 pc, (c) 0.02 pc, and (d) 0.01 pc. The green dashed line represents the Eddington accretion rate  $\dot{m}_E$  for the initial mass of the BH. The purple line represents the critical condition that bifurcates the key mechanisms for the growth of the BH. The brown dot-dashed line represents the lower limit of gas density for the occurrence of merger within  $10^8$  yr, which is roughly estimated from Fig. 6 in Tagawa et al. (2015).

roughly sound velocity in  $2 \times 10^5$  yr. Thereafter, the BH interacts gravitationally with other smaller BHs. Since the grown-up BH has a larger Schwarzschild radius, the merger condition (8) is liable to be satisfied. Shortly after the total accretion, two BHs approaching the heaviest BH merge by the gravitational wave radiation. Then, several BHs are left without merger in the system until the end of simulation. Hence, the merger of all BHs into one BH is hard to occur in a type D.

## 4 MERGER VERSUS ACCRETION

### 4.1 Critical condition

A significant measure for the growth of massive BHs is provided by the condition under which the predominant mechanism of the BH growth is bifurcated between the merger and the accretion. In Fig. 10, resultant merger types are summarized with the contribution of the accreted mass  $m_{\text{ac}}$  to the final mass  $m_{\text{fin}}$  at the end of simulations. This figure shows that the fractions of accreted mass are a steep function in a two parameter plane of  $\epsilon$  and  $n_{\text{gas}}$ , depending on the extension of BH distributions. This behavior comes from the fact that the Hoyle-Lyttleton-type accretion rate is a nonlinear function of mass as shown in equation (6) and

therefore diverges at the finite time as

$$m_i = \frac{1}{m_0^{-1} - \alpha t}, \quad (11)$$

where  $m_0$  is the initial mass and  $\alpha = \epsilon 4\pi G^2 m_{\text{H}} n_{\text{gas}} / (C_s^2 + v_i^2)^{3/2}$ .

In the environments of low gas density, if the velocity of each BH is near to  $C_s$ ,  $t_{\text{DF}}$  and  $t_{\text{ac}}$  are not dependent on the BH density,  $\rho_{\text{BH}}$ , furthermore, both  $t_{\text{DF}}$  and  $t_{\text{ac}}$  have the same dependence on  $n_{\text{gas}}$ . Therefore, the critical accretion efficiency,  $\epsilon_c$ , above which the accretion mass becomes predominant, is expected to be  $\epsilon_c = \text{const}$ , irrespective of  $\rho_{\text{BH}}$  and  $n_{\text{gas}}$ . Here, to assess  $\epsilon_c$ , we employ the average of accretion mass-to-final mass ratios,  $m_{\text{ac}}/m_{\text{fin}}$ . Also, the numerical results used in this assessment are restricted to those in low-density regions of  $n_{\text{gas}} < 10^8 \text{ cm}^{-3}$ . Then, we derive  $\epsilon_c$  by linear interpolation of  $m_{\text{ac}}/m_{\text{fin}}$  between  $\max\{\log \epsilon\}$  for  $2m_{\text{ac}} < m_{\text{fin}}$  and  $\min\{\log \epsilon\}$  for  $2m_{\text{ac}} > m_{\text{fin}}$ . As a result, we find  $\epsilon_c = 6 \times 10^{-3}$ . This value is broadly consistent with the condition that the accretion timescale is a few hundred times shorter than the timescale for the merger of ten BHs, as discussed in Tagawa et al. (2015).

On the other hand, in high-density regions, the boundary of accretion-dominant branches is depending on  $n_{\text{gas}}$  and  $r_{\text{typ}}$ . To derive the dependence of the critical accretion efficiency on  $n_{\text{gas},c}$ , we use the results in high-density regions of  $n_{\text{gas}} \geq 10^8 \text{ cm}^{-3}$  for a given BH density, say  $r_{\text{typ}}$ .



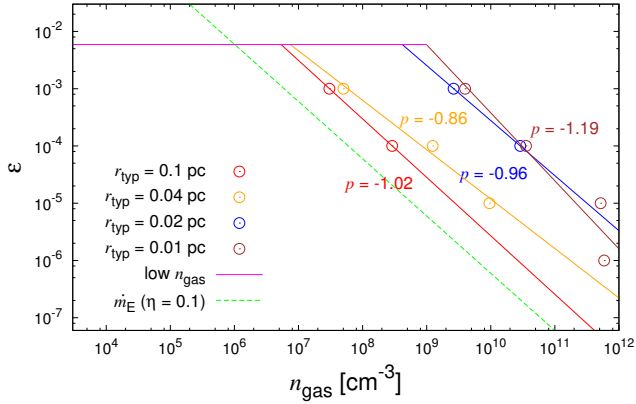


**Figure 11.** The critical accretion efficiency,  $\epsilon_c$ , as a function of ambient gas density  $n_{\text{gas}}$ . Red, orange, blue, and brown plots represent the critical condition in high-density regions for  $r_{\text{typ}} = 0.1, 0.04, 0.02,$  and  $0.01$  pc, respectively. Red, orange, blue, and brown lines represent the curves fitted by  $n_{\text{gas},c} = ae^p$  for  $r_{\text{typ}} = 0.1, 0.04, 0.02,$  and  $0.01$  pc. Pink line represents the critical condition in low-density regions. The green dashed line represents the Eddington accretion rate  $\dot{m}_E$ .

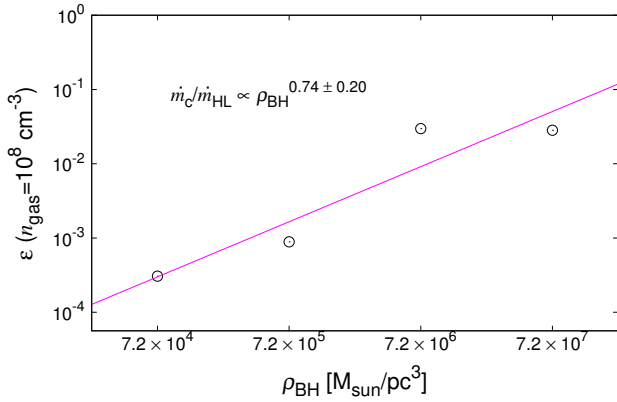


**Figure 12.** The critical accretion efficiency,  $\epsilon_c$ , as a function of  $\rho_{\text{BH}}$ , for  $n_{\text{gas}} = 10^8 \text{ cm}^{-3}$ . A straight line is the fitting using a power law of  $\epsilon(n_{\text{gas}} = 10^8 \text{ cm}^{-3}) = a\rho_{\text{BH}}^q$ .

In Fig. 11, we show the critical accretion efficiency,  $\epsilon_c$ , as a function of  $n_{\text{gas}}$ . As shown in Fig. 11, the dependence on  $n_{\text{gas}}$  seems similar, almost irrespective of  $r_{\text{typ}}$ . Actually, if we assume a power law as  $\epsilon_c = an_{\text{gas}}^p$ , we can fit the results with  $p = -1.01 \pm 0.07$ , by linear interpolation of  $m_{\text{ac}}/m_{\text{fin}}$  between  $\max\{\log n_{\text{gas}}\}$  for  $2m_{\text{ac}} < m_{\text{fin}}$  and  $\min\{\log n_{\text{gas}}\}$  for  $2m_{\text{ac}} > m_{\text{fin}}$ . Next, we determine the dependence on  $\rho_{\text{BH}}$ . In Fig. 12, we show the critical accretion efficiency as a function of  $\rho_{\text{BH}}$ . The dependence seems to be well fitted by a power law form again. If we assume  $\epsilon_c = an_{\text{gas}}^{-1.01}\rho_{\text{BH}}^q$ , we find the best fit value as  $q = 0.74 \pm 0.20$ .

Combining the results for low and high gas density cases, the critical accretion efficiency is given as

$$\epsilon_c = \begin{cases} 6 \times 10^{-3} & \text{for } n_{\text{gas}} \lesssim 10^8 \text{ cm}^{-3} \\ 2 \times 10^{-3} \left(\frac{n_{\text{gas}}}{10^8 \text{ cm}^{-3}}\right)^{-1.0} \left(\frac{\rho_{\text{BH}}}{10^6 M_{\odot} \text{ pc}^{-3}}\right)^{0.74} & \text{for } n_{\text{gas}} \gtrsim 10^8 \text{ cm}^{-3}. \end{cases} \quad (12)$$

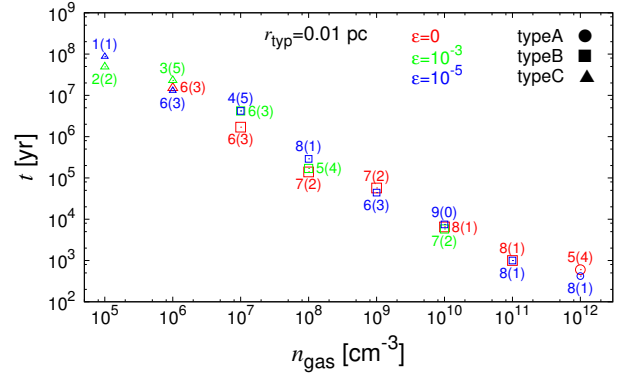


**Figure 13.** First merger time as a function of gas number density  $n_{\text{gas}}$  for  $r_{\text{typ}} = 0.01$  pc in the case that the merger dominantly contribute to the first growth of the BHs. Red, green, and blue plots represent the merger time in the cases of no accretion ( $\epsilon = 0$ ), intermediate accretion ( $\epsilon = 10^{-3}$ ), and lower accretion ( $\epsilon = 10^{-5}$ ), respectively. Also, circle, square, and triangle symbols represent the types A, B, and C mergers, respectively. The number (in parentheses) described beside each symbol represent the number of merged (escaped) BHs.

The efficiency of  $6 \times 10^{-3}$  corresponds to a super-Eddington accretion rate with the Eddington ratio of  $\sim 10$ . The relation of equation (12) can be basically understood by a condition from timescales as  $t_{\text{DF}} \sim t_{\text{ac}}$ . Supposing  $v \leq Cs$ , this condition leads to  $\epsilon_c = \text{const}$  in a low-density limit and  $\epsilon_c \propto n_{\text{gas}}^{-3/2}\rho_{\text{BH}}$  in a high-density limit. The difference in the power law of the critical condition between the numerical results and an analytic estimate may come partially from mass accretion in supersonic phases and also from the gradual transition from low-density regions to high-density regions. Equation (12) shows that if  $\rho_{\text{BH}}$  is lower ( $r_{\text{typ}}$  is larger), then the critical accretion efficiency becomes lower in high density environments of  $n_{\text{gas}} \gtrsim 10^8 \text{ cm}^{-3}$ . It is noted that as shown in §2.2, the accretion efficiency is constrained by the radiation pressure if  $\epsilon > 0.1$ . However, the critical accretion efficiency given by (12) is considerably smaller than  $\epsilon = 0.1$ , and therefore is not affected by the limitation of accretion rate due to the radiation pressure.

The present simulations show that if the BH merger precedes the gas accretion, all BHs are likely to merge into one large BH. This may be relevant to the fact that just one BH resides in the center of a massive galactic bulge. On the other hand, if the gas accretion precedes the BH merger, multiple BHs are left in the system. Intriguingly, a lot of stellar mass ( $\sim 50M_{\odot}$ ) BHs are found in the center of M31 (Barnard et al. 2014). Although the origin of such a lot of stellar-mass BHs is not unveiled yet, multiple BHs can be left if the collective growth of a BH is driven by mass accretion.

## 4.2 Effects of Boundary Conditions

In this paper, we have assumed the finite gas mass in a sphere. Here, we investigate the influences of this treatment on the merger timescale and mechanisms. In Fig. 13, we compare the merger timescale for no accretion ( $\epsilon = 0$ , red symbols) to that for intermediate accretion ( $\epsilon = 10^{-3}$ , green

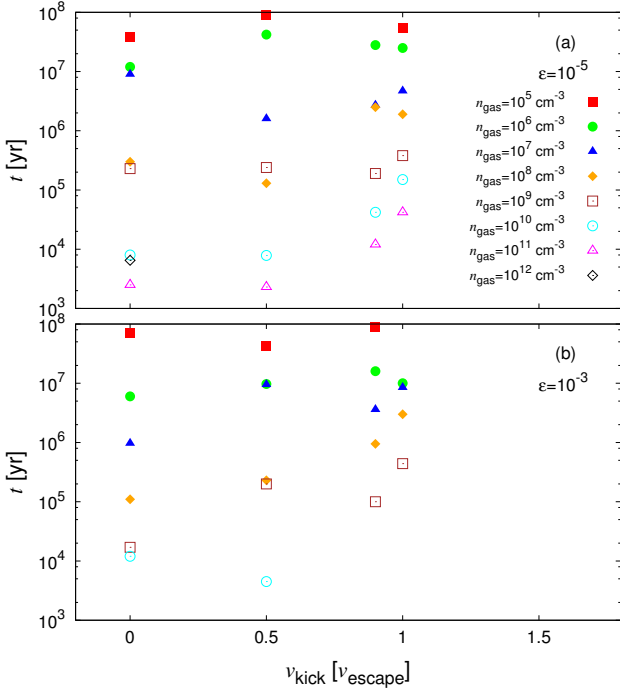


**Figure 14.** The averaged merger time as a function of the kick velocity in the cases of  $r_{\text{typ}} = 0.01$  pc and  $v_{\text{kick}} \leq v_{\text{escape}}$ . Filled red squares, green circles, blue triangles, orange diamonds, open brown squares, blue circles, magenta triangles, and black diamonds represent the merger time for  $n_{\text{gas}} = 10^5, 10^6, 10^7, 10^8, 10^9, 10^{10}, 10^{11},$  and  $10^{12} \text{ cm}^{-3}$ , respectively. Panel (a) presents the results for the case of lower accretion ( $\epsilon = 10^{-5}$ ), while panel (b) for intermediate accretion ( $\epsilon = 10^{-3}$ ).

symbols) or for lower accretion ( $\epsilon = 10^{-5}$ , blue symbols), in the cases in which the merger dominantly contributes to the first growth of BHs. In those cases, it is found that the boundary conditions of gas distributions do not bring significant influence on the merger timescale within uncertainties of a factor of 2. Furthermore, the merger mechanisms are also not influenced by the finiteness of the gas mass and the gas accretion.

Since the total mass in the system is finite, escapers due to the slingshot mechanism emerge. The averaged number of escapers is  $2 \sim 3$  in the present system with  $M_{\text{gas,tot}} = 10^5 M_{\odot}$ . The number of escaped BHs is expected to increase in a shallower gravitational potential. Therefore, in order for multiple BHs to merge via type B or C mechanism, a deep potential is requisite.

### 4.3 Effect of Recoil Kick

In this section, we consider the effect of the recoil kick due to the anisotropic emission of gravitational wave radiation. The recoil velocity depends sensitively on the magnitudes of BH spins and the alignment with the orbital angular momentum of a BH binary.

To investigate the effect of the recoil kick, we perform the simulations incorporating the recoil in the case of  $r_{\text{typ}} = 0.01$  pc. In these simulations, we give the kick

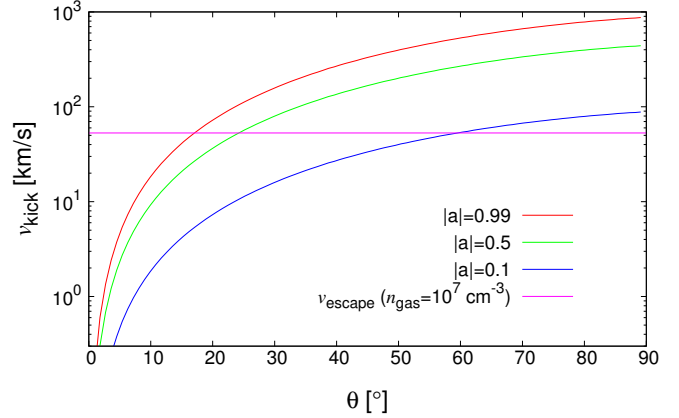


**Figure 15.** The averaged kick velocity as a function of the angle ( $\theta$ ) between the spin of one BH and the angular momentum of the binary in the cases that two BHs have the same masses and spin magnitude, and the spin direction of another BH is the same as the direction of the angular momentum of the binary. Red, green, and blue lines represent the results for BH spin magnitude of  $|a_1| = |a_2| = 0.99, 0.5,$  and  $0.1$ , respectively. The pink line denotes the escape velocity for a gas cloud of  $n_{\text{gas}} = 10^7 \text{ cm}^{-3}$ .

velocity  $v_{\text{kick}}$  as 0, 0.5, 0.9, 1.0, 1.1, and 1.5 times escape velocity  $v_{\text{escape}}$ . Also, the number of BHs is set to be five to spare a computational cost. As expected, we find that if  $v_{\text{kick}} \leq 1.0 \times v_{\text{escape}}$ , the merged BH stays in the system, while in the cases of  $v_{\text{kick}} \geq 1.1 \times v_{\text{escape}}$ , the successive BH merger is halted due to the escape of the merged BH. In Fig. 14, we show the averaged merger time as a function of the kick velocity for  $v_{\text{kick}} \leq v_{\text{escape}}$ . From this figure, the merger timescale for  $v_{\text{kick}} \sim v_{\text{escape}}$  is almost the same as that for  $v_{\text{kick}} = 0$  in low gas density cases as  $n_{\text{gas}} < 10^8 \text{ cm}^{-3}$ . This is because the merger timescale is almost irrespective of the initial extension of BH distributions in low BH density cases (Tagawa et al. 2015). On the other hand, in high gas density cases ( $n_{\text{gas}} \geq 10^8 \text{ cm}^{-3}$ ), the merger timescale for  $v_{\text{kick}} \sim v_{\text{escape}}$  is longer by about one order of magnitude than that for  $v_{\text{kick}} = 0$  km/s. From these results, the critical accretion rate is expected to be reduced by about one order of magnitude in high gas density regions, if the non-negligible recoil velocity is incorporated.

Next, we assess the probability that the kick velocity exceeds the escape velocity for each gas density. Here, we assume perfectly random orientation and magnitude of BH spins for equal mass BHs. To derive the probability, we calculate  $10^7$  sets of BH spins. The model of the recoil velocity is employed from Campanelli et al. (2007), and we give the two angle  $\xi$  and  $\Theta_0$  in equation (1) of Campanelli et al. (2007) as  $\xi = 90^\circ$  and  $\Theta_0 = 0^\circ$ . In Table. 1, the escape velocity for each gas density and the probability of  $v_{\text{kick}} > v_{\text{escape}}$  are shown. From this table, we expect that in a first-generation object ( $n_{\text{gas}} \sim 10^7 \text{ cm}^{-3}$ ), about 90 percent of merged BHs may escape from the system. Thus, the effect of recoil velocity can reduce the BH merger rate significantly. This estimate is the results for the random directions and magnitudes of BH spins. On the other hand, if BH spins and the orbital angular momentum are aligned with each other, the probability may change. Considering the binary formation, we can suppose that the directions of

**Table 1.** The escape velocity and probability for each gas number density in the cases of random spins and equal mass BHs.

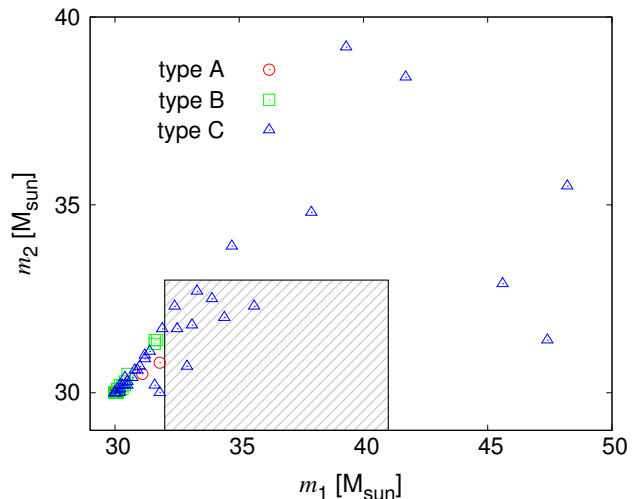
$n_{\text{gas}}$ ( $\text{cm}^{-3}$ )	$v_{\text{escape}}$ (km/s)	$P(v_{\text{kick}} > v_{\text{escape}})$ (%)
$10^5$	24.6	95.6
$10^6$	36.1	93.4
$10^7$	53.0	90.2
$10^8$	77.7	85.3
$10^9$	114	78.0
$10^{10}$	167	67.2
$10^{11}$	246	52.5
$10^{12}$	361	35.8

BH spins are similar to the direction of the angular momentum of the binary. To make a simple estimate, we change the direction of the spin ( $\mathbf{a}_1$ ) of one BH, assuming that the direction of the other BH spin ( $\mathbf{a}_2$ ) is the same as the orbital angular momentum direction, and the spin magnitude is the same ( $|\mathbf{a}_1| = |\mathbf{a}_2|$ ). The resultant kick velocities are averaged over  $10^5$  sets of the random azimuthal angles between the projected direction of  $\mathbf{a}_1$  to the orbital plane of the binary and the infall direction at a merger. Fig. 15 shows the kick velocity as a function of  $\theta$ . As a result, in the cases of the rapidly rotating BHs ( $|\mathbf{a}_1| = |\mathbf{a}_2| = 0.99$ ) mergers, the averaged kick velocity exceeds the escape velocity in  $\theta > 16.2^\circ$ . This means that if  $\theta$  is randomly given from  $0^\circ$  to  $90^\circ$ , about 82 percent will escape and 18 percent stay in the system. According as the BH spin magnitude decreases, the escape fraction decreases. Thus, it is expected that the escape probability of a merged BH stemming from a binary becomes lower than that for the cases of the random spins. Furthermore, Natarajan & Pringle et al. (1998) have suggested that the spins of BHs are aligned with the outer accretion disk typically within  $\sim 10^5 - 10^6$  yr due to the Bardeen-Petterson effect, although the large uncertainty in the viscosity may vary the alignment timescale (Volonteri et al. 2007).

#### 4.4 Merger in GW150914

Very recently, the Laser Interferometer Gravitational-Wave Observatory (LIGO) has detected the gravitational wave event, GW150914, as a result of the merger of a  $\sim 30 M_\odot$  BH binary (Abbott et al. 2016). This binary is composed of a  $36_{-4}^{+5} M_\odot$  and  $29_{-4}^{+4} M_\odot$  BH, and the final BH mass is  $62_{-4}^{+4} M_\odot$ . These observations demonstrate that binary stellar-mass black hole systems exist and they can merge within the cosmic time. The masses of a binary BH in the GW150914 event are close to our assumption of the initial BH mass.<sup>1</sup> Based on the present numerical simulations, obviously the merger event in GW150914 is not an accretion-

<sup>1</sup> After the present calculations were almost completed, the detection of gravitational waves in GW150914 was reported. Hence, we have not explored whether BHs with initial mass lower than  $30 M_\odot$  can account for the BH binary in GW150914. This will be studied in a forth-coming paper.

**Figure 16.** The masses in a binary just before the first merger in each run. Red circle, green square and blue triangle plots represent type A, B and C mergers. The masses inferred from GW150914 with their uncertainties are indicated by the hatched regions.

driven merger, since the final mass is not so high as expected in an accretion-driven merger. In Figure 16, the masses in a binary just before the first merger in our simulations are shown. We find that in several sets of parameters, the masses in a binary match those in GW150914 within their uncertainties. All the mergers in these parameters are driven by three-body interactions (type C) in the range of gas density from  $n_{\text{gas}} = 10^5 \text{ cm}^{-3}$  to  $10^{10} \text{ cm}^{-3}$ . The density of  $n_{\text{gas}} = 10^{5-8} \text{ cm}^{-3}$  corresponds to high density interstellar clouds, and  $n_{\text{gas}} \gtrsim 10^8 \text{ cm}^{-3}$  corresponds to the galactic center regions of  $\lesssim 1$  pc. Also, these three body-driven mergers are accompanied by highly super-Eddington accretion, and the mass of a few  $M_\odot$  is accreted before mergers. Such gas accretion might produce electromagnetic emission associated with gravitational wave events.<sup>2</sup>

## 5 CONCLUSIONS

In this paper, we have explored the merger of multiple BHs systems under background gas distributions, incorporating dynamical friction and gas accretion. For the purpose, we have performed highly accurate post-Newtonian numerical simulations taking into account such general relativistic effects as the pericenter shift and gravitational wave emission. Consequently, we have found the followings.

(1) The dominant mechanisms for the growth of BHs are varied according to the gas accretion rate  $\dot{m}$ , the BH density  $\rho_{\text{BH}}$ , and the gas number density  $n_{\text{gas}}$ . The merger mechanisms are classified into a gas drag-driven merger

<sup>2</sup> It was reported that a weak transient source above 50 keV was detected 0.4 s after the GW150914 event by Fermi Gamma-ray Burst Monitor (GBM) (Connaughton et al. 2016). However, it is pointed out that the GBM transient event is very unlikely associated with the GW150914 (Greiner et al. 2016; Xiong 2016).

(type A), an interplay-driven merger (type B), a three body-driven merger (type C), or an accretion-driven merger (type D).

(2) In a type A, B, or C merger, all BHs can merge eventually into one heavy BH, if the BH merger precedes the gas accretion. However, in a type D, the merger of all BHs into one BH is hard to occur, leaving several BHs around a primary BH.

(3) We have derived the critical accretion rate  $\dot{m}_c$ , below which the BH growth is predominantly promoted by mergers. The  $\dot{m}_c$  is fitted as

$$\frac{\dot{m}_c}{\dot{m}_{\text{HL}}} = \begin{cases} 6 \times 10^{-3} & \text{for } n_{\text{gas}} \lesssim 10^8 \text{ cm}^{-3} \\ 2 \times 10^{-3} \left( \frac{n_{\text{gas}}}{10^8 \text{ cm}^{-3}} \right)^{-1.0} \left( \frac{\rho_{\text{BH}}}{10^6 M_{\odot} \text{pc}^{-3}} \right)^{0.74} & \text{for } n_{\text{gas}} \gtrsim 10^8 \text{ cm}^{-3}. \end{cases} \quad (13)$$

Note that the effect of the recoil kick may reduce the critical accretion rate by about one order of magnitude for high gas density regions. Also, since our analytic prescriptions of the gas effects do not take the inhomogeneity of gas distributions into account, our simulations may overestimate the effects of the mass accretion and the dynamical friction by gas.

(4) The recoil kick due to the anisotropic emission of gravitational wave radiation is important to estimate the event rate of BH mergers. We have estimated that roughly ninety percent of merged BHs can escape from a first-generation object, if the directions and magnitudes of BH spins are completely random. The escape probability is reduced, if BH spins and the orbital angular momentum are aligned with each other.

(5) Supposing the gas and BH density based on the recent simulations on the first star formation, the BH merger proceeds before the significant mass accretion, if the accretion rate is lower than  $\sim 10$  Eddington accretion rate.

(6) The merger of a binary BH system in GW150914 is most likely to be driven by three-body encounters accompanied by a few  $M_{\odot}$  of gas accretion.

In this paper, we do not consider the dynamics of the gas. However, the effect of the gas dynamics may affect the merger or accretion mechanism. We will investigate the influence of the effect of the gas dynamics on the BH merger in the future.

## ACKNOWLEDGMENTS

We thank Taihei Yano for valuable discussions. Numerical computations and analyses were carried out on Cray XC30 and computers at Center for Computational Astrophysics, National Astronomical Observatory of Japan, respectively. This research was also supported in part by Interdisciplinary Computational Science Program in Center for Computational Sciences, University of Tsukuba, and Grant-in-Aid for Scientific Research (B) by JSPS (15H03638).

## REFERENCES

- Aasi J., et al., 2013, *Phys. Rev. D.*, 87, 022002  
 Abbott B. P., et al., 2006, *Phys. Rev. D.*, 73, 062001  
 Abbott B. P., et al., 2016, *Phys. Rev. Lett.*, 116, 061102  
 Abbott B. P., et al., 2016, *ApJ*, 818, L22  
 Abramowicz M. A., Czerny B., Lasota J. P., Szuszkiewicz E., 1988, *ApJ*, 332, 646  
 Alvarez M. A., Wise J. H., Abel T., 2009, *ApJ*, 701, L133  
 Aso Y., Michimura Y., Somiya K., Ando M., Miyakawa O., Sekiguchi T., Tatsumi D., Yamamoto H., 2013, *PhRvD*, 88, 043007  
 Barnard R., Garcia M. R., Primini F. Murray S. S., 2014, *ApJ*, 791, 33  
 Bergin E. A., Snell R. L., Goldsmith P. F., 1996, *ApJ*, 460, 343  
 Berti E., Cardoso V., Will C. M., 2006, *Phys. Rev. D.*, 73, 064030  
 Bondi H., Hoyle F., 1944, *MNRAS*, 104, 273  
 Campanelli M., Lousto C. O., Zlochower Y., Merritt D., 2007, *PhRvL*, 98, 1102  
 Connaughton V., et al., 2016, arXiv, arXiv:1602.03920  
 Djorgovski S. G., Courbin F., Meylan G., Sluse D., Thompson D., Mahabal A., Glikman E., 2007, *ApJ*, 662, L1  
 Escala A., Larson R., Coppi P., Mardones D., 2004, *ApJ*, 507, 765  
 Escala A., Larson R., Coppi P., Mardones D., 2005, *ApJ*, 630, 152  
 Fan X. et al., 2001, *AJ*, 122, 2833  
 Farina E. P., Montuori C., Decarli R., Fumagalli M., 2013, *MNRAS*, 431, 1019  
 Greif T. H., Springel V., White S. D. M., Glover S. C. O., Clark P. C., Smith R. J., Klessen R. S., Bromm V., 2011, *ApJ*, 737, 75  
 Greiner J., Burgess J. M., Savchenko V., Yu H.-F., 2016, arXiv, arXiv:1606.00314  
 Haiman Z., 2013, in Wiklind T., Mobasher B., Bromm V., eds, *Astrophysics and Space Science Library*, Vol. 396, The First Galaxies. Springer-Verlag, Berlin, p. 293  
 Hanamoto K., Ioroi M., Fukue J., 2001, *PASJ*, 53, 105  
 Heger A., Woosley S. E., 2002, *ApJ*, 567, 532  
 Hirano S., Hosokawa T., Yoshida N., Umeda H., Omukai K., Chiaki G., Yorke H. W., 2014, *ApJ*, 781, 60  
 Hoyle F., Lyttleton R. A., 1939, *Proc. Camb. Phil. Soc.*, 35, 405  
 Iwasawa M., Funato Y., Makino J., 2006, *ApJ*, 651, 1059  
 Kormendy J., Ho L. C., 2013, *ARA&A*, 51, 511  
 Kupi G., Amaro-Seoane P., Spurzem R., 2006, *MNRAS*, 371, 45  
 Kurk J. D., et al., 2007, *ApJ*, 669, 32  
 Liu X., Shen Y., Strauss M. A., 2011, *ApJ*, 736, L7  
 Lück H., et al., 2006, *CQGra*, 23, S71  
 Makino J. Aarseth S., 1992, *PASJ*, 44, 141  
 Merritt D., Poon M. Y., 2004, *ApJ*, 606, 788  
 Milosavljevic M., Couch S. M., Bromm V., 2009, *ApJ*, 696, 146  
 Mortlock D. J., et al., 2011, *Nature*, 474, 616  
 Namekata D., Umemura M., 2016, *MNRAS*, 460, 980  
 Natarajan P., Pringle J. E., 1998, *ApJ*, 506, L97  
 Omukai K., 2000, *ApJ*, 534, 809  
 Ostriker E. C., 1999, *ApJ*, 513, 252  
 Schawinski K., Urry M., Treister E., Simmons B., Natarajan

- Jan P., Glikman E., 2011, *ApJ*, 743, L37  
Sesana A., Haardt F., Madau P., Volonteri M., 2005, *ApJ*, 623, 23  
Susa H., 2013, *ApJ*, 773, 185  
Susa H., Hasegawa K., Tominaga N., 2014, *ApJ*, 792, 32  
Tagawa H., Umemura M., Gouda N., Yano T., Yamai Y., 2015, *MNRAS*, 451, 2174  
Tanaka T., Haiman Z., 2009, *A & A*, 696, 1798  
Tanikawa A., Umemura M., 2011, *MNRAS*, 728, 31  
Tanikawa A., Umemura M., 2014, *MNRAS*, 440, 652  
Umemura M., 2001, *ApJ*, 560, L29  
Umemura M., Loeb A., Turner E. L., 1993, *ApJ*, 419, 459  
Umemura M., Susa H., Hasegawa K., Suwa T., Semelin B., 2012, *PTEP*, 2012, 01A306  
Volonteri M., Bellovary J., 2012, *Rep. Prog. Phys.*, 75, 124901  
Volonteri M., Rees M. J., 2005, *ApJ*, 633, 624  
Volonteri M., Sikora M., Lasota J.-P., 2007, *ApJ*, 667, 704  
Volonteri M., Silk J., Dubus G., 2015, *ApJ*, 804, 148  
Watarai K., Fukue J., Takeuchi M., Mineshige S., 2000, *PASJ*, 52, 133  
Wu X.-B., et al., 2015, *Nature*, 518, 512  
Wyithe J. S. B., Loeb A., 2003, *ApJ*, 590, 691  
Xiong S., 2016, arXiv, arXiv:1605.05447  
Yajima H., Li Y., Zhu Q., Abel T., 2015, *ApJ*, 801, 52